Annealing kinetics of electrodeposited lithium dendrites

Asghar Aryanfar,[1,a)] Tao Cheng,[2] Agustin J. Colussi,[1] Boris V. Merinov,[2] William A. Goddard III,[2] and Michael R. Hoffmann[1]
[1]*Linde Center for Global Environmental Science, California Institute of Technology, Pasadena, California 91125, USA*
[2]*Materials and Process Simulation Center, California Institute of Technology, Pasadena, California 91125, USA*

(Received 24 June 2015; accepted 7 August 2015; published online 1 October 2015)

The densifying kinetics of lithium dendrites is characterized with effective activation energy of $E_a \approx 6-7$ kcal mol^{-1} in our experiments and molecular dynamics computations. We show that heating lithium dendrites for 55 °C reduces the representative dendrites length $\overline{\lambda}(T,t)$ up to 36%. NVT reactive force field simulations on three-dimensional glass phase dendrites produced by our coarse grained Monte Carlo method reveal that for any given initial dendrite morphology, there is a unique stable atomic arrangement for a certain range of temperature, combined with rapid morphological transition (~10 ps) within quasi-stable states involving concurrent *bulk* and *surface* diffusions. Our results are useful for predicting the inherent structural characteristics of lithium dendrites such as dominant coordination number. © *2015 AIP Publishing LLC.* [http://dx.doi.org/10.1063/1.4930014]

I. INTRODUCTION

During last decade, the wireless revolution and the need for harnessing intermittent renewable power sources have created an exponential demand for energy storage devices such as long-lasting and high energy density batteries.[1] Particularly, pure lithium (Li^0) is the battery anode material with the ideal energy density of 3862 mAh/g, which could drastically satisfy this demand. However, it has very high propensity to grow *dendrites* during consecutive recharging periods.[2] This phenomenon eventually leads to short-circuiting, overheating the cell, and possible ignition of the organic electrolyte as well as creating isolated *dead lithium* crystals during discharge periods.[3] Therefore, although the ongoing research aims to develop novel Li-air, Li-S, and flow battery technologies, the dendrite problem remains as a critical and challenging issue for rechargeability and lifetime.[4–6]

Researchers have investigated the role of charging method,[7] current density,[8,9] electrode surface morphology[10–13] and impurity,[14,15] solvent and electrolyte chemical composition,[16–18] electrolyte concentration,[8,19] electrode surface passivation,[20] powder electrodes,[21] and adhesive polymers[22] on dendrite growth. The unconventional techniques used for dendrites characterization includes NMR[23] and MRI.[24] Current dendrite continuum modeling frameworks are helpful, but they involve simplifying assumptions that may have fallen short of capturing the atomic-scale essentials of dendrite growth.[25–27]

Temperature is a highly accessible parameter with the foremost important effect on kinetics. It has been found that cycling at higher temperatures (from −50 °C up to 40 °C) can, on average, cause more frequent short-circuiting events up to a factor of 2.[28] Other results show that the increasing cell temperature enhances the ionic mobility in favor of dendritic inception and growth.[29] The reports indicate that the higher temperatures extend the ion depletion layer length, which is in agreement with temperature dependence of reaction rates.[8,9,30] The probability of ionic reduction in the electrode surface is also correlated directly to the temperature.[31] In contrast, imposing higher temperatures reduces dendrite growth rate relative to the electrode surface and could result in more uniform deposition.[32] Although all those approaches are helpful, it is apparent that further progress in tackling this crucial issue should accrue from a full understanding of kinetics of dendrites for Li-metal electrode applications.

In our recent work, we have found that applying the gradient of temperature during electrodeposition has a destructive effect on growing dendrites.[20] In this paper, we assess the activation energy of lithium dendrites by using a new experimental setup and by developing a reactive force field (ReaxFF) framework. We also investigate the possible annealing pathways on a basic atomic arrangement. This study could open routes for intelligent cyclic thermal treatment of dendrites to avoid the eventual short-circuiting of the cell during operation.

II. EXPERIMENTS

We have manually fabricated novel cells for *in situ* observation and measurement of electrolytic Li^0 deposits (Fig. 1(a)).[33] Round disk electrodes (area = 1.6 cm^2) were punched from a Li^0 foil (Aldrich, 99.9%, 0.38 mm thick) that had been cleaned of oxide layers by scraping with a blade and dimethyl carbonate (DMC) in a glove box sparged with argon gas (H_2O, O_2 < 0.5 ppm). The disk electrodes were mounted on silicone gaskets and pressed against a poly(methylmethacrylate) (PMMA) electrode separator that kept them $L = 3.175$ mm apart. The electrolyte 1M $LiClO_4$ (Aldrich, battery grade, 99.99%, dried for 24 h at 90 °C under vacuum) solution in propylene carbonate (PC) (Aldrich, 99.7%

a)Author to whom correspondence should be addressed. Electronic mail: aryanfar@caltech.edu. Tel.: +1 (626) 395-8736. Fax: +1 (626) 395-8535.

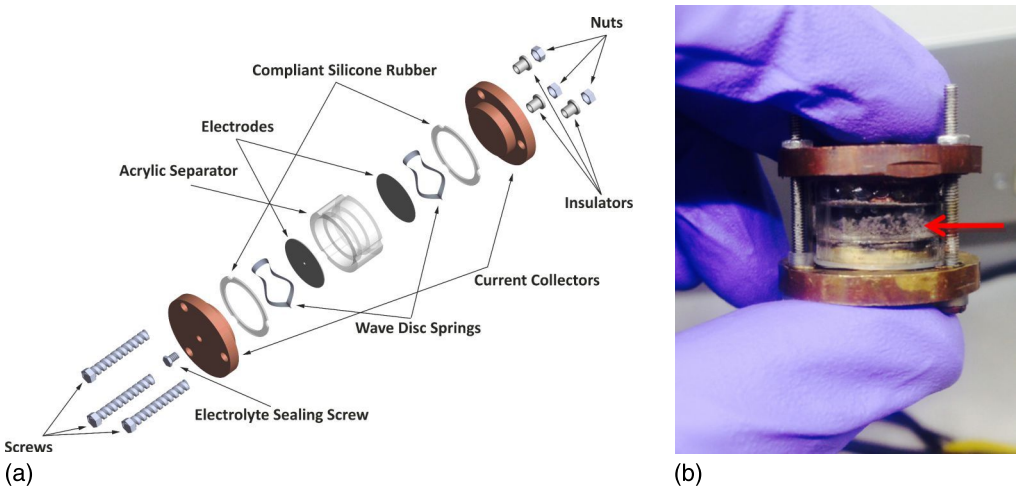

FIG. 1. (a) Component-level view of the cell. (b) Lithium dendrites observed by naked eye from the PMMA separator.

FIG. 2. Naked-eye observation of *in situ* lithium dendrites created at $i = 2$ mA cm^{-2} for $t = 24$ h (a) before and (b) after submerging in the oil bath of $T = 78$ °C for $t = 48$ h. The *filled* area fraction has been reduced from 64% to 41%.

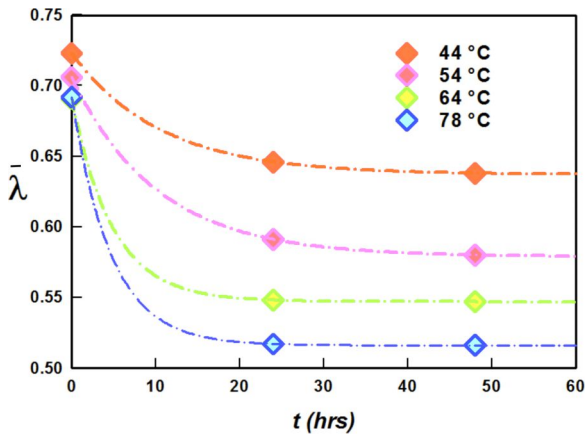

FIG. 3. Dendrite measures $\overline{\lambda}(T,t)$ versus bath temperature for 4 various post-charge bath temperatures. The initial dendrites are produced with charging rate of $i = 2$ mA cm^{-2} for $t = 24$ h ($Q = 48$ mAh).

anhydrous) was injected into the cell, whereupon the opening was sealed with a Teflon plug.

The fabricated cells were charged in ambient condition using Bio-logic instruments (SP-50, VSP). The cells were disconnected and rinsed with isopropyl alcohol. The optical observations were done on the post-charge anode surface. Subsequently, the cells were submerged in various oil bath temperatures. The cells were taken out every 12 h and microscopic observations were done on their periphery. A typical naked-eye observation of lithium dendrites before and after submerging in oil bath is shown in Fig. 2.

Forty-five equidistant measurements were done on the periphery of each cell via Leica M205FA microscope. The dendrite lengths typically spanned from 200 μm to 3000 μm enabling to observe them with naked eye (Fig. 1(b)). The normalized dendrite lengths to the interelectrode distance with their multiplicities normalized to the total counts in specified length ranges $[\lambda_i, p_i]$ were measured in series of experiments. The figure of merit is defined as the average weighted lengths of measured dendrites normalized to interelectrode distance L,

$$\overline{\lambda}(T,t) = \frac{1}{L}\sum_{i=1}^{n} \lambda_i p_i, \tag{1}$$

where

$$\sum_{i=1}^{n} p_i = 1. \tag{2}$$

The time-dependent results are demonstrated in Fig. 3.

III. COMPUTATIONAL SIMULATIONS

We have utilized the ReaxFF method to describe the interactions of deposited Li^0 atoms. The energy of the system can be expressed as a function of bond order as

$$\begin{aligned} E_{system} = {} & E_{bond} + E_{lp} + E_{over} + E_{under} \\ & + E_{val} + E_{pen} + E_{C2} + E_{triple} + E_{tors} \\ & + E_{conj} + E_{H-bond} + E_{vdw} + E_{Coloumb}. \end{aligned} \tag{3}$$

Details of terms in (3) can be found in the literature.[34,35] ReaxFF force fields are trained against extensive atomic structures including charge, bond dissociation energy, geometry of finite moles, different crystal phases (cell parameters and relative stabilities), and energy data. For

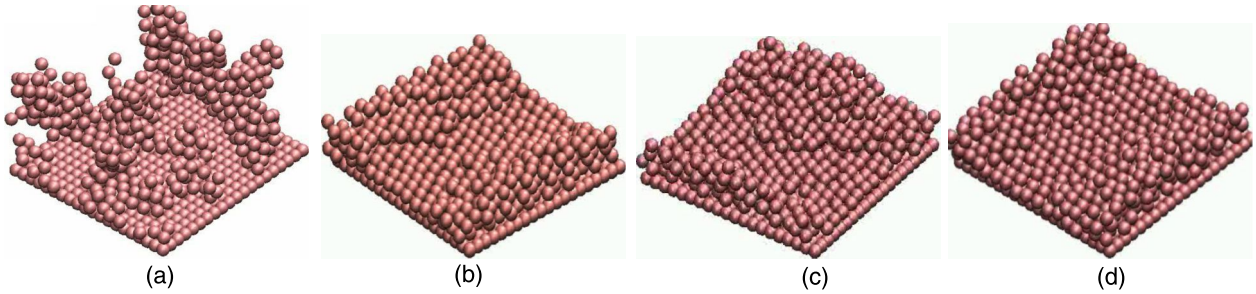

FIG. 4. (a) Initial optimized dendrite glass phase from CG-MC method. Final morphologies after 200 ps NVT simulations at 317 K (b), 337 K (c), and 357 K (d) are demonstrated.

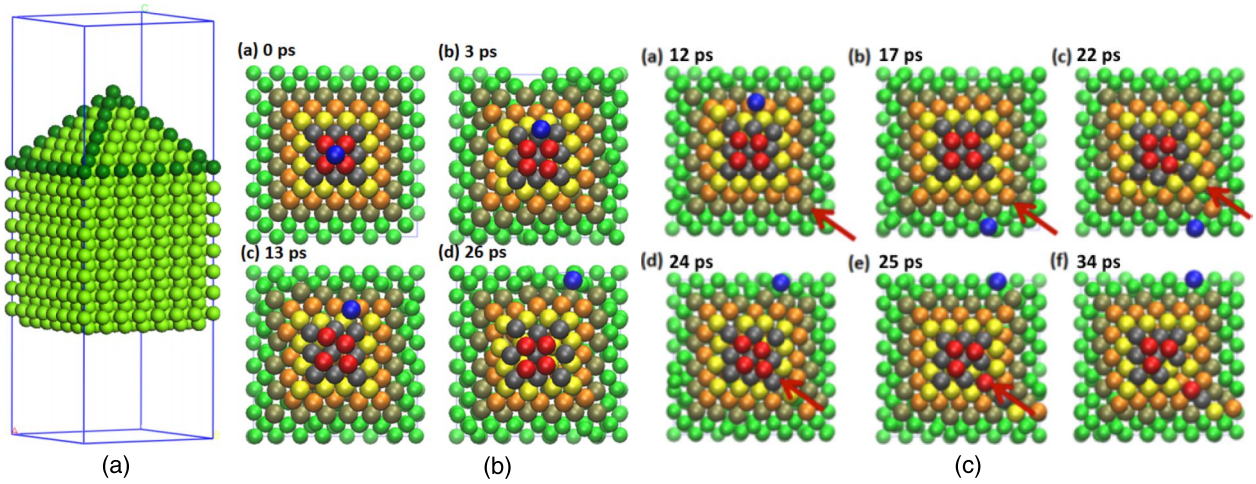

FIG. 5. (a) The pyramid model. (b) SD mechanism (blue atom). (c) BD mechanism (red arrow) at 250 K.

TABLE I. Model parameters.

x and y dimensions	24.57 Å
z dimension	38.61 Å
Cube layers	7×7×15
Tip layers	15
Domain width	24.57×24.57 Å
Domain height	10.53 Å
Simulation time	200 ps
Simulation time step	0.25 fs
Damping constant	12.5 fs

Li metal, the training set includes Li_2^+ bond dissociation curves, crystal structures of different crystalline phases (body-centered cubic (BCC), face-centered cubic (FCC), hexagonal closed packed (HCP), diamond and simple cubic (SC)) and corresponding equations of state (EOS), atomization energy, and energy differences of these crystals. We also considered the surface energy of (100), (110), and (111) of BCC Li. The trained ReaxFF well reproduces the surface energy values obtained from the quantum mechanics (QM) calculations. The list of parameters is included in the supplementary material 1.[36]

The initial 3D glass phase morphology of dendrites is generated from our previously developed coarse grain (CG) framework,[20] which utilized the same experimental parameters for Li and 1M $LiClO_4$/PC solution. In order to avoid the system to be trapped in local potential minima, we optimized the structures using steepest descent algorithm followed by conjugate gradient algorithm and finally damped dynamics methods (each 1000 steps).[37] The Nudged elastic band (NEB) calculations were carried out followed by the hill-climbing NEB simulations to determine the transition barrier and to trace the path between the 6 optimized replicas from the initial and final structures (each 1000 steps).[38–40]

The energy minimization was carried out using the ReaxFF with imposing fixed bottom layers for Li. The optimized structure is a glass phase of the Li crystal (100) surface as shown in Fig. 4(a). The NVT simulations were carried out at temperatures ranging from 317 K to 357 K to investigate the temperature effect on elimination of dendrites. In most cases, the Li dendrite quickly collapsed upon the start and 3–5 atoms thick layers were formed after 200 ps of simulation time. Figs. 4(b)-4(d) visualize the structural arrangements. The obtained structures show ordered Li atoms, which is a feature of crystalline phase. To ensure reliable results, the simulations have been performed for 4 different initial glass phase morphologies. The average elevation of 10 highest atoms is considered as the measure, λ_{10}, which is tracked against time (Figs. 6(b) and 6(c)). A sample movie can be found in the supplementary material 2.[36]

In order to study the dendrite collapse in more detail, we have idealized the initial atomic arrangement to a pyramid-like morphology that consists of 15 layers of Li bulk ($7 \times 7 \times 15$) substrate and 6 layers of the Li pyramid ending up at single atom tip (Fig. 5, Table I). The facets of the pyramid correspond

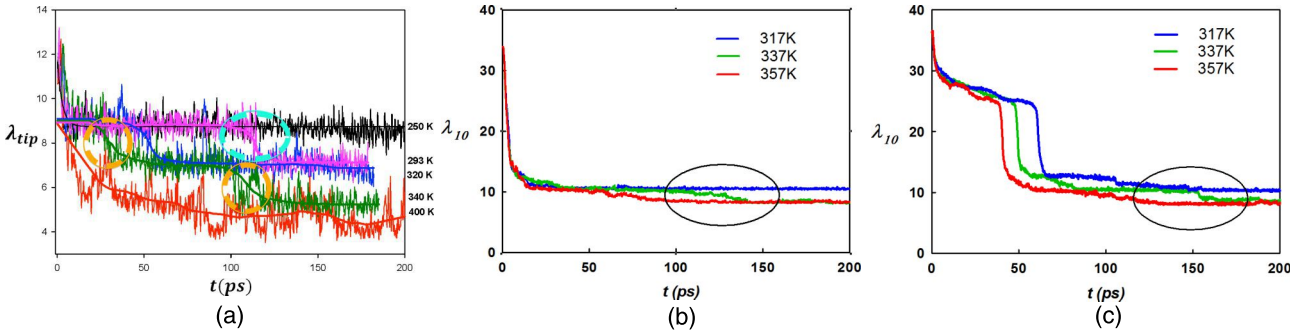

FIG. 6. (a) Simulation of $\lambda_{tip}(T,t)$ (Å) in pyramid model. The encircled cyan and orange regions indicate 1 and 2 rapid transitions between two metastable states. ((b) and (c)) $\lambda_{10}(T,t)$ for 2 simulated initial glass phase dendritic morphologies from MC-CG method. The transition between two quasi-stable states is evident in the encircled regions.

to the (110) surface. Since the dendrites have amorphous nature with all possible orientations, the surface can be arbitrarily chosen. A 30 Å vacuum space is built to avoid the interactions between the slab and its translationally identical images. Since nano-scale structures usually exhibit very low melting point comparing with that for bulk phase, we fixed the bottom ten layers to avoid the unrealistic melting. Each layer ($L_1, L_2, \ldots$ from the top) is colored differently to track the movements. The tip atom elevation, that is the first atom to move due to relatively low coordination number, is tracked versus time (Fig. 6(a)).

Using the optimized structure, we relaxed the x and y directions at 50 K to adjust the pressure to 1 bar by expanding or compressing the box along the x and y directions. The obtained structures were then heated up to target temperatures using the Nose-Hover temperature control.[41]

IV. RESULTS AND DISCUSSION

Our simulations and experiments clearly indicate that the representative height for dendrites is temperature and time dependent (i.e., $\overline{\lambda} = \overline{\lambda}(T,t)$) and fits well within first-order kinetics paradigm,

$$\overline{\lambda}(T,t) = \overline{\lambda}_0 \exp(-k(T)t), \tag{4}$$

where

$$k(T) = k(T_0)\exp\left(\frac{-E_a}{k_B}\left(\frac{1}{T} - \frac{1}{T_0}\right)\right). \tag{5}$$

Hence, we can extract the effective activation energy E_a for dendrites from (5). We have differentiated two dominant reduction mechanisms for the tip model.

A. Surface diffusion (SD)

The adatom drops off from the top with energy barrier starting from 5.2 kcal/mol ($L_1 \rightarrow L_2$), followed by diffusion with increased barriers of 10.1 kcal/mol ($L_2 \rightarrow L_3$), to 11.2 kcal/mol ($L_3 \rightarrow L_4$). Corresponding movie is included in the supplementary material 3.[36]

B. Bulk diffusion (BD)

The adatom creates a vacancy with energy barriers starting from 9.7 kcal/mol, followed by vacancy diffusion with a very small barrier of 2.5 kcal/mol. This makes it easy for the vacancies to diffuse from the bottom to the top, which may lead to the structure collapse. The supplementary material 4 shows the movie for this phenomenon.[36]

Although the diffusion energy barrier of BD is smaller than SD, which makes BD the prevalent mechanism, it is highly possible that both of those mechanisms occur simultaneously due to the small difference. Also, as expected, the atoms in the corners (i.e., lowest coordination number) moved sooner (Table II).

The experimental results revealed that typically shorter dendrites were formed at higher imposed temperatures (Fig. 3) which is consistent with the result of our previous studies.[28,32] It is also apparent that average dendrite length, $\overline{\lambda}$, versus time t converges to a temperature dependent asymptote $\overline{\lambda}_\infty(T)$. On the simulations side, the pyramid setup is in a metastable phase and given enough time, it will finally transform into flat surface. At low temperature, a fraction of rearrangement will occur, which traps the system in local equilibrium. Increasing temperature can largely decrease this possibility since followed by increasing the average coordination number.

Although the time scale of experiments and computations is vastly different, the initial rate of variation in dendrite's measure $-\frac{d\overline{\lambda}(T,t)}{dt}$ remains as an appropriate measure for their correlation.

The energy barrier for the movement of the tip atom on the (110) surface is consistent with another set of our QM calculations of the migration barrier of 3 kcal/mol for a Li atom on the (100) surface. The energy barrier for BD is 9.7 kcal/mol, which is higher than for SD ($L_1 \rightarrow L_2$), but slightly lower than for the other pathways, which means it is highly possible to occur. The activation energy barrier obtained from fitting is 7.2 kcal/mol (Fig. 7(a)) in consistence with the NEB simulations (Fig. 7(b)). These results correlate with

TABLE II. Energy barriers (E_a) calculated from NEB method between 4 layers.

Path	E_a (kcal/mol)
$L_1 \rightarrow L_2$ (SD)	5.2
$L_2 \rightarrow L_3$	10.1
$L_3 \rightarrow L_4$	11.2
$L_6 \rightarrow$ *bulk* (BD)	9.7
Vacancy	2.5

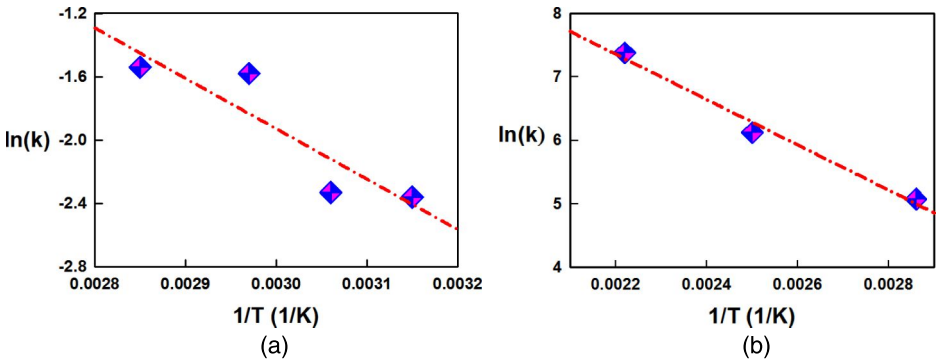

FIG. 7. First order Arrhenius kinetics fitting of (a) experimental (b) computational results. The acquired activation energies are 7.1 kcal/mol and 6.3 kcal/mol, respectively.

density functional theory (DFT) studies of lithium diffusion on the (001) and (011) surfaces.[42]

V. CONCLUSIONS

In this paper, we quantified the thermal annealing kinetics of lithium dendrites in our experiments and simulations. We produced the lithium dendrites in laboratory experiments and measured their temperature dependent reduction via a novel design and method. On the other hand, we created lithium dendrites using our CG-MC framework and by training ReaxFF framework for lithium, we predicted their effective thermal relaxation energy barrier. The acquired effective activation energy of 7.1 kcal/mol from the experiments matches well with the corresponding value of 6.3 kcal/mol from simulations. The surface diffusion of low-coordinated atoms and bulk diffusion was ascribed as the dominant mechanisms for thermal relaxation of lithium dendrites. The results have potential for predicting the internal structural properties of amorphous dendrites such as the dominant coordination number, porosity, branching characteristics, and material dependency. Further work along these lines is underway.

ACKNOWLEDGMENTS

The authors would like to gratefully thank the financial support from Bill and Melinda Gates Foundation, Grant No. OPP1069500, on environmental sustainability and, in part, by Bosch Energy Research Network, Grant No. 13.01.CC11. The help from undergraduate student Mark Lorden and discussions with graduate student Daniel Brooks are also acknowledged.

[1]M. Armand and J. M. Tarascon, Nature **451**, 652 (2008).
[2]L. Vitos, A. V. Ruban, H. L. Skriver, and J. Kollar, Surf. Sci. **411**, 186 (1998).
[3]A. Aryanfar, D. J. Brooks, A. J. Colussi, and M. R. Hoffmann, Phys. Chem. Chem. Phys. **16**, 24965 (2014).
[4]W. Xu, J. L. Wang, F. Ding, X. L. Chen, E. Nasybutin, Y. H. Zhang, and J. G. Zhang, Energy Environ. Sci. **7**, 513 (2014).
[5]B. Huskinson, M. P. Marshak, C. Suh, S. Er, M. R. Gerhardt, C. J. Galvin, X. Chen, A. Aspuru-Guzik, R. G. Gordon, and M. J. J. Aziz, Nature **505**, 195 (2014).
[6]J. B. Goodenough and Y. Kim, J. Power Sources **196**, 6688 (2011).
[7]A. Aryanfar, D. Brooks, B. V. Merinov, W. A. Goddard III, A. J. Colussi, and M. R. Hoffmann, J. Phys. Chem. Lett. **5**, 1721 (2014).
[8]C. Brissot, M. Rosso, J. N. Chazalviel, and S. Lascaud, J. Electrochem. Soc. **146**, 4393 (1999).
[9]A. D. P. F. Orsini, B. Beaudoin, J. M. Tarascon, M. Trentin, N. Langenhuisen, E. D. Beer, and P. Notten, J. Power Sources **76**, 19 (1998).
[10]X. H. Liu, L. Zhong, L. Q. Zhang, A. Kushima, S. X. Mao, J. Li, Z. Z. Ye, J. P. Sullivan, and J. Y. Huang, Appl. Phys. Lett. **98**, 183107 (2011).
[11]C. Monroe and J. Newman, J. Electrochem. Soc. **151**, A880 (2004).
[12]T. Nishida, K. Nishikawa, M. Rosso, and Y. Fukunaka, Electrochim. Acta **100**, 333 (2013).
[13]C. P. Nielsen and H. Bruus, preprint arXiv:1505.07571 (2015).
[14]K. J. Harry, D. T. Hallinan, D. Y. Parkinson, A. A. MacDowell, and N. P. Balsara, Nat. Mater. **13**, 69 (2014).
[15]J. Steiger, D. Kramer, and R. Monig, J. Power Sources **261**, 112 (2014).
[16]P. C. Howlett, D. R. MacFarlane, and A. F. Hollenkamp, J. Power Sources **114**, 277 (2003).
[17]N. Schweikert, A. Hofmann, M. Schulz, M. Scheuermann, S. T. Boles, T. Hanemann, H. Hahn, and S. Indris, J. Power Sources **228**, 237 (2013).
[18]R. Younesi, G. M. Veith, P. Johansson, K. Edström, and T. Vegge, Energy Environ. Sci. **8**, 1905 (2015).
[19]C. Brissot, M. Rosso, J. N. Chazalviel, and S. Lascaud, J. Power Sources **81**, 925 (1999).
[20]A. Aryanfar, D. J. Brooks, A. J. Colussi, B. V. Merinov, W. A. Goddard III, and M. R. Hoffmann, Phys. Chem. Chem. Phys. **17**, 8000 (2015).
[21]I. W. Seong, C. H. Hong, B. K. Kim, and W. Y. Yoon, J. Power Sources **178**, 769 (2008).
[22]G. Stone, S. Mullin, A. Teran, D. Hallinan, A. Minor, A. Hexemer, and N. Balsara, J. Electrochem. Soc. **159**, A222 (2012).
[23]R. Bhattacharyya, B. Key, H. L. Chen, A. S. Best, A. F. Hollenkamp, and C. P. Grey, Nat. Mater. **9**, 504 (2010).
[24]S. Chandrashekar, N. M. Trease, H. J. Chang, L.-S. Du, C. P. Grey, and A. Jerschow, Nat. Mater. **11**, 311 (2012).
[25]J. N. Chazalviel, Phys. Rev. A **42**, 7355 (1990).
[26]C. Monroe and J. Newman, J. Electrochem. Soc. **150**, A1377 (2003).
[27]D. R. Ely, A. Jana, and R. E. García, J. Power Sources **272**, 581 (2014).
[28]H. E. Park, C. H. Hong, and W. Y. Yoon, J. Power Sources **178**, 765 (2008).
[29]J. Diggle, A. Despic, and J. M. Bockris, J. Electrochem. Soc. **116**, 1503 (1969).
[30]C. Brissot, M. Rosso, J. N. Chazalviel, and S. Lascaud, J. Power Sources **94**, 212 (2001).
[31]A. J. Bard and L. R. Faulkner, *Electrochemical methods, fundamentals and applications* (Wiley, New York, 1980), Vol. 2.
[32]R. Akolkar, J. Power Sources **246**, 84 (2014).
[33]A. Aryanfar, "Method and device for dendrite research and discovery in batteries," U.S. patent application 14/201,979 (September 11, 2014).
[34]A. C. T. van Duin, S. Dasgupta, F. Lorant, and W. A. Goddard, J. Phys. Chem. A **105**, 9396 (2001).
[35]K. Chenoweth, A. C. T. van Duin, and W. A. Goddard, J. Phys. Chem. A **112**, 1040 (2008).
[36]See supplementary material at http://dx.doi.org/10.1063/1.4930014 for the list of ReaxFF parameters; the NVT simulation movie NVT of a sample glass-phase lithium dendrite created by CG-MC method; for surface diffusion mechanism; and for bulk diffusion mechanism.
[37]D. Sheppard, R. Terrell, and G. Henkelman, J. Chem. Phys. **128**, 134106 (2008).
[38]B. J. Berne, G. Cicootti, and D. F. Coker, "Classical and quantum dynamics in condensed phase simulations" (1998), p. 385.
[39]G. Henkelman, B. P. Uberuaga, and H. Jónsson, J. Chem. Phys. **113**, 9901 (2000).
[40]G. Henkelman and H. Jónsson, J. Chem. Phys. **113**, 9978 (2000).
[41]G. J. Martyna, D. J. Tobias, and M. L. Klein, J. Chem. Phys. **101**, 4177 (1994).
[42]M. Jäckle and A. Groß, J. Chem. Phys. **141**, 174710 (2014).